Hindawi
Shock and Vibration
Volume 2019, Article ID 8592578, 13 pages
https://doi.org/10.1155/2019/8592578

Research Article

Study on the Resonant Suppression of Electrohydraulic Servo Shaking Table of a 2-Mass Dynamic System

Tao Wang and Jinchun Song

School of Mechanical Engineering and Automation, Northeastern University, Shenyang 110819, Liaoning, China

Correspondence should be addressed to Tao Wang; molili94@126.com

Received 12 July 2018; Revised 18 September 2018; Accepted 21 November 2018; Published 2 January 2019

Academic Editor: Mario Terzo

Since the load of electrohydraulic servo shaking table is an elastic load, there is a mutual coupling effect that exists between the experimental object and the shaking table, forming the resonance to weaken the dynamic characteristics, and producing resonant peak and resonant valley in the bandwidth required by the system, in which the amplitude is often larger than the stability range of acceleration's amplitude. In this paper, the mathematical modeling of hydraulic power mechanism in a two-mass dynamic system is established based on electrohydraulic servo shaking table, yielding the frequency characteristic curve in accordance with the transfer function of the model. A multifrequency adaptive notch filter based on the least mean square algorithm is proposed to suppress the resonance, and the suppression effect of the resonance is simulated and verified in line with various values of load stiffness. Finally, the power spectrum is used to demonstrate the effectiveness of the multifrequency adaptive notch filter in the resonant suppression.

1. Introduction

In recent years, the shaking table has become a critical test tool in engineering research and plays a crucial role in environmental simulation, e.g., aerospace, automobile, building, and earthquake simulation, especially in modern times, which requires high reliability of the system. The hydraulic vibration test also has become an essential way of modern industrial reliability test. With the improvement of product reliability and the standard of vibration damping, the servo shaking table directly impacts the accuracy of test. Thus, the system's reliability is becoming increasingly demanding [1, 2].

When the elastic load test is performed on the shaking table, the oil liquid in the closed chamber is compressed, and the leakage is equivalent to a "hydraulic spring." In the meantime, the shaking table test system has a coupling relation with the elastic load, reducing the dynamic characteristics of the system, and a corresponding resonant peak and the resonant valley will exist in the bandwidth required by the system [3, 4]. Due to the existence of this resonant phenomenon, the stability of the system becomes worse, which cannot meet the requirements of system stability. For the vibration test system, how to eliminate the coupling effect on the frequency characteristic of the shaking table's acceleration, to restrain the resonance and make the frequency characteristic of the shaking table meet the standard of vibration test, has become a critical subject of the present research.

The existence of the resonance will not only impact the working performance and the service life of the components but also produce noise and other types of pollution and sometimes even damage the components and sealing devices. The harmonic oscillation will occur if the natural frequency of the hydraulic system happens to the frequency of the pressure oscillation simultaneously. This type of oscillation suddenly strikes in the short time which will not only be reduced by the influence of resonance, whereas it will in turn increase. Under this short-time impact, the pipe, component, and sealing device of the hydraulic system will be higher than the working pressure and make them to be seriously damaged to affect normal work after several times

of pressure shock. Besides, the impact of pressure shock and oscillation also lead to noise pollution in the workspace [5, 6].

In comparison with the mechanical system and the power system, the resonant suppression method based on the servo system is quite limited by its high requirement and precision. Thus, the new suppression methods should adapt to meet the performance requirements of electrohydraulic servo system. Resonance of the brake pressure control system is a fluid-solid coupling vibration caused by the joint action of the brake control valve and the brake system pipe. Given this, Lu et al. put forward the method of changing the parameters of the pipeline, the back pressure of the system, and the brake control valve in the brake system, capable of effectively restraining the resonant phenomenon of the aircraft brake system [7]. Fu et al. had analyzed the low-frequency resonance of an aero hydraulic engine and designed a feedforward controller composed of low pass filter, PD compensation, and feedforward correction, which successfully suppressed the resonance and improved the overall amplitude and phase margin of the system [8]. Tomoki et al. proposed a parameter identification method to model electrohydrostatic actuators as two-mass resonant systems, and the self-resonant cancellation technique was implemented to suppress the effect of resonance [9]. The notch filters were applied by Younkin in fixed frequency resonances to stabilize the servo drives with unacceptable machine dynamics, and this frequency selective feedback control technique also stabilized the servo drives with unacceptable machine dynamics [10]. Cao et al. put forward a method to suppress the resonance of the excited cylinder by setting an external damper between the two working chambers of the excited cylinder to form a bypass leakage to improve the hydraulic damping ratio [11].

In the servo system, change of natural frequency, load characteristic, and additional characteristic can change the frequency and amplitude of the resonance, so the adaptive algorithm is put forward to suppress the resonance. A developed method for resonant suppression based on adaptive filtered x-least mean square algorithm was presented by Wang et al., which obtained the resonance iteratively and reduced the significant resonant oscillations using a finite impulse response filter, which was adapted by the least mean square error principle [12]. Kang and Kim proposed the method of an adaptive digital notch filter that could identify the resonant frequency of the actuator quickly and adjust automatically its center frequency [13]. The resonant online suppressing algorithm based on adaptive IIR notch filter was proposed by Li et al. in accordance with the application requirements; the resonant frequency of the system was online estimated and then the frequency parameters of notch filter was adjusted online by using a recursive least-squares algorithm [14]. Bahn et al. brought a new algorithm for estimating the resonant frequency of adaptive notch filters in servo systems, which was proportional to the difference in the estimated frequency and actual frequency and allowed to select the estimation parameters independent from the value of resonant frequencies [15]. To improve the performance of the servo system to overcome the influence of the previously neglected elastic components, the adaptive notch filter was employed by Yang et al. for online resonant suppression; thus, the characteristics of the mechanical resonance could be identified quickly, and the parameters of the notch filter could be automatically adjusted by the identification results [16].

In brief, though there are numerous methods to suppress the resonance, the suppression of the experimental platform based on shaking table is not much, which should keep the real-time suppression effect when this method is applied in the servo system. The rest of the paper is arranged as follows: in Section 2, the frequency characteristics of the shaking table are provided based on the power mechanism. In Section 3, the theory of adaptive notch filter methods for resonance suppression is proposed, and the multifrequency adaptive notch filter is analyzed based on LMS. In Section 4, the simulation results of the resonance suppression in line with different values of load stiffness and the power spectrum of the electrohydraulic servo system are presented. The effectiveness and superiority are verified by the comparison of the suppression resonant effect between the multifrequency adaptive notch filter and the digital filter. At last, Section 5 is the conclusion.

2. Electrohydraulic Servo Shaking Table

2.1. The Equipment. The block diagram of the shaking table system is shown in Figure 1. It is a uniaxial shaking table with supply pressure of 8 MPa. A hydraulic cylinder is controlled by a two-stage servo valve. The stroke of the cylinder is ±25 mm, and the diameters of its rod and piston are Φ36 mm and Φ50 mm, respectively. The system is under acceleration control with a frequency range from 0 Hz to 125 Hz to reproduce the desired shaking response.

The three A/D channels are mainly used to receive displacement, acceleration signals, and speed signals obtained by conditioning, and all of them are converted into digital signals and transmitted to the upper computer for analysis and processing in the system. A D/A channel is used to convert the control signals of the system into analog signals and input them into the shaking table system, so as to realize the conversion between the signals of the system [17].

2.2. Analysis of the Hydraulic Power Mechanism. In Figure 2, the load part is abstracted into an elastic load, and the effect of friction on the load is ignored. Under the action of elastic load, the electrohydraulic servo system is a two-degree-of-freedom model [18].

Before modeling the servo system, it is necessary to make some following assumptions: without considering leakage and compressibility of oil, the zero-opening four-side slide valves should be used as the type, in which throttles of the hydraulic can be matched with each other, and they are completely in symmetrical distribution. Because the

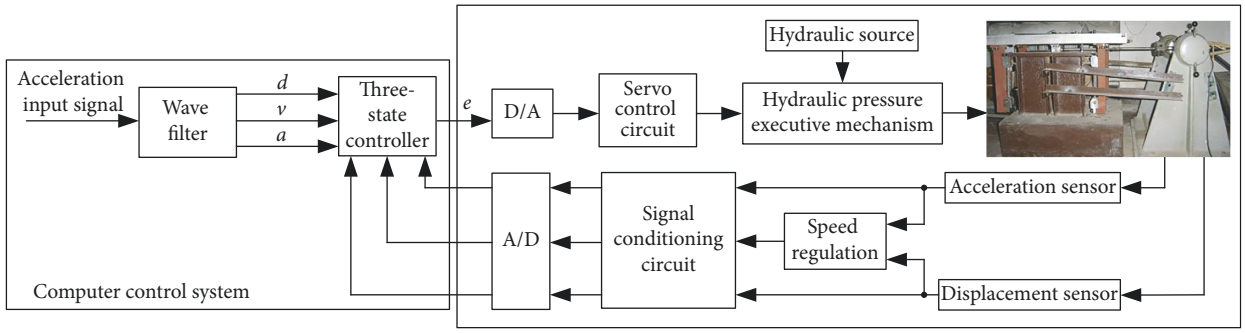

Figure 1: Control system of shaking table.

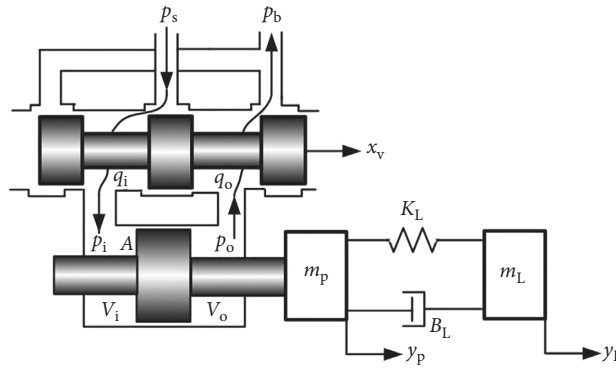

Figure 2: Schematic diagram of hydraulic power mechanism.

constant pressure variable oil source is adopted, the oil pressure is kept constant. So, the oil return pressure is at zero [19]. The equation is shown as follows:

$$q_L = K_q x_v - K_c p_L. \tag{1}$$

The following assumptions are shown: connection among the components of the servo system remains symmetrical; it does not consider the effect of friction in the hydraulic pipeline [20]. Under this condition, the equation is established as follows:

$$q_L = A\frac{dy_p}{dt} + C_{tp}p_L + \frac{V_t}{4\beta_e}\cdot\frac{dp_L}{dt}. \tag{2}$$

The right-hand side of Equation (2) is made up of three parts. One is the flow used to act on the piston rod which plays a leading role in providing power to the hydraulic cylinder for the action of the piston rod. The second is the total leakage flow of the system that consists mainly of two components of internal leakage and external leakage, which form a hydraulic servo system. The third is the total compression flow, which is manifested in the compressibility of hydraulic oil to composing the compression loss of the system, but it can be ignored.

The equation of force balance of two degrees of freedom is established, and its characteristics are analyzed by linearization method. Considering the influence of load force, viscous damping force, and inertia force, the force balance equation can be obtained as follows:

$$Ap_L = m_p\frac{d^2y_p}{dt^2} + B_L\frac{dy_p}{dt} + K_L y_p - B_L\frac{dy_L}{dt} - K_L y_L, \tag{3}$$

$$m_L\frac{d^2y_L}{dt^2} = B_L\frac{dy_p}{dt} + K_L y_p - B_L\frac{dy_L}{dt} - K_L y_L. \tag{4}$$

Equations (1)–(4) can be organized by Laplace transformation:

$$\frac{Y_L}{X_V} = \frac{K_q}{A}\frac{B_L s + K_L}{D(s)}, \tag{5}$$

$$\begin{aligned} D(s) = {} & \frac{m_p m_L}{K_h}s^5 + \left[\frac{B_L(m_p + m_L)}{K_h} + \frac{K_{ce}m_p m_L}{A^2}\right]s^4 \\ & + \left[m_L + \frac{K_{ce}B_L(m_p + m_L)}{A^2} + \frac{K_L(m_p + m_L)}{K_h}\right]s^3 \\ & + \left[B_L + \frac{K_{ce}K_L(m_p + m_L)}{A^2}\right]s^2 + K_L s. \end{aligned} \tag{6}$$

Using equations (3) and (4), we obtain the following equation:

$$\frac{Y_L}{Y_p} = \frac{B_L s + K_L}{m_L s^2 + B_L s + K_L}. \tag{7}$$

Using equations (5) and (7), equation (8) can be summarized as follows:

$$\frac{Y_p}{X_V} = \frac{K_q}{A} \frac{m_L s^2 + B_L s + K_L}{D(s)}. \quad (8)$$

From the above, it can be seen that when the vibration test of the elastic load is carried out, the coupling action of the hydraulic system constitutes a resonant system. The comprehensive stiffness of the system is made up of two parts in series, one is the stiffness of the hydraulic spring K_h, which is caused by the compressibility of the fluid. The second is the load stiffness K_L, which is determined by the load condition of the load. After being connected in series, the composite stiffness is less than K_h and K_L.

Comparison of equation (8) shows that the elastic system increases two links than the inertial system, one is the oscillation link which can cause the emergence of the resonant peak, and the other is the two-order differential link which can cause the appearance of the resonant valley. Therefore, equation (8) causes the resonance induced in the system bandwidth, and the amplitude of the resonance exceeds the required range due to the smaller damping. The conventional resonant suppression strategy, such as improving the comprehensive resonant frequency and the comprehensive damping ratio, is difficult to obtain accurate coupling parameters because of the uncertainty and nonlinearity of the coupling characteristics. The suppression effect of the resonance is often very limited, which cannot meet the demand of tolerance limit. Therefore, it is necessary to study the nonlinear control strategy with adaptive function to suppress the coupling effect of elastic load on the acceleration frequency characteristics of shaking table.

The effective working area of the piston rod A is calculated as follows:

$$A = \frac{\pi(D^2 - d^2)}{4} = 945.6 \times 10^{-6}\ \mathrm{m}^2, \quad (9)$$

where d represents the diameter of the piston rod and D represents the inner diameter of the hydraulic cylinder. L value is ±200 mm which represents the hydraulic cylinder in stroke. The total volume of the oil tank and the pipeline oil can be obtained as

$$V_t = AL = 3.78 \times 10^{-4}\ \mathrm{m}^3. \quad (10)$$

Compressed liquid of hydraulic cylinder can be approximately a linear equivalent total hydraulic spring stiffness, so K_h is

$$K_h = \beta_e A^2 \left(\frac{1}{V_i} + \frac{1}{V_o}\right). \quad (11)$$

And when the piston rod is at the middle of the position, the value is

$$K_h = \frac{4\beta_e A^2}{V_t} = 6.53 \times 10^6\ \mathrm{N/m}, \quad (12)$$

where the damping ratio is the smallest value. So the parameters based on the hydraulic system power mechanism are shown as Table 1.

Table 1: Parameters based on the hydraulic system power mechanism.

Piston diameter D (mm)	50
Piston rod diameter d (mm)	36
Piston effective area A (m^2)	945.6×10^{-6}
Stroke of hydraulic cylinder L (mm)	±200
Equivalent volume modulus of elasticity β_e (MPa)	690
Pipe diameter d_1 (m)	0.01
Equivalent mass of load inertia m_p (kg)	100
Elastic load quality m_L (kg)	100
Hydraulic spring stiffness K_h (N/m)	6.53×10^6
Servo valve gain K_q (m^3/s/A)	2×10^{-2}
Flow-pressure coefficient K_{ce} (m^3/s/Pa)	3×10^{-12}
Viscous damping coefficient of the piston and load B_L (N/(m/s))	80

2.3. The Frequency Analysis. From the above section, it can be seen that the elastic system increases the oscillating link and the two-order differential link compared with the inertial system, which leads to the emergence of resonance. In order to determine the relationship between the frequency value of the resonant peak and valley and the natural frequency of the dynamic mechanism, the two-degree-of-freedom equivalent vibration model is established that ignores the damping effect, and the dynamic differential equations are established, respectively:

$$m_p \frac{d^2 y_p}{dt^2} + (K_L + K_h) y_p - K_L y_L = 0, \quad (13)$$

$$m_L \frac{d^2 y_L}{dt^2} - K_L y_P + K_L y_L = 0. \quad (14)$$

Equations (13) and (14) can be expressed in matrix form as

$$\begin{bmatrix} m_p & 0 \\ 0 & m_l \end{bmatrix} \begin{bmatrix} y_p \\ y_L \end{bmatrix} + \begin{bmatrix} K_h + K_L & -K_L \\ -K_L & K_L \end{bmatrix} \begin{bmatrix} y_p \\ y_L \end{bmatrix} = \begin{bmatrix} 0 \\ 0 \end{bmatrix}. \quad (15)$$

The natural frequency of the two-degree-of-freedom system can be obtained by solving the following characteristic equation.

$$\left| \begin{bmatrix} K_h + K_L & -K_L \\ -K_L & K_L \end{bmatrix} - \omega^2 \begin{bmatrix} m_p & 0 \\ 0 & m_l \end{bmatrix} \right| = 0. \quad (16)$$

The expansions of equation (16) can be obtained as follows:

$$m_L m_p \omega^4 - \left(K_h m_L + K_L m_L + K_L m_p\right)\omega^2 + K_h K_L = 0. \quad (17)$$

Thus, two natural frequencies can be solved, respectively.

$$\omega_0^2 = \frac{K_h m_L + K_L m_L + K_L m_p - \sqrt{\left(K_h m_L + K_L m_L + K_L m_p\right)^2 - 4K_h K_L m_L m_p}}{2m_L m_p},$$
$$\omega_p^2 = \frac{K_h m_L + K_L m_L + K_L m_p + \sqrt{\left(K_h m_L + K_L m_L + K_L m_p\right)^2 - 4K_h K_L m_L m_p}}{2m_L m_p}, \tag{18}$$

where ω_0 is the composite frequency and ω_p is the frequency of resonant peak. Equation (6) can be converted into the following form:

$$D(s) = \frac{1}{\omega_L^2 \omega_h^2} s^5 + \left(\frac{2\varsigma_L}{\omega_L \omega_x} + \frac{\varsigma_x \omega_x}{\omega_L^2 \omega_h^2}\right) s^4 + \left(\frac{1}{\omega_L^2} + \frac{2\varsigma_x \varsigma_L}{\omega_x \omega_L} + \frac{1}{\omega_x^2}\right) s^3 + \left(\frac{2\varsigma_L}{\omega_L} + \frac{\varsigma_x}{\omega_x}\right) s^2 + s, \tag{19}$$

where ω_L is the frequency of the resonant valley, $\omega_L = \sqrt{K_L/m_L}$, $\varsigma_L = B_L/2\sqrt{K_L m_L}$, ω_x is the coupling frequency, $\omega_x = \sqrt{K_h/(m_p + m_L)}$, $\varsigma_x = (2K_{ce}/A)\sqrt{(\beta_e/V_t)(m_p + m_L)}$, and ω_h is the natural frequency of the power mechanism, $\omega_h = \sqrt{K_h/m_p}$.

But the actual value is not exactly equal to the calculated value. The reason is that the damping of the hydraulic system is small, so the damping has little influence on the comprehensive natural frequency, which can be used to calculate the integrated fixed frequency.

3. Multifrequency Adaptive Notch Filter

Adaptive notch technology is derived from adaptive noise cancellation, which sets a sinusoidal signal as a reference signal to counteract every component in narrowband noise. When the sine wave is used as the reference input, it can eliminate the main spectrum component at the center of the narrow band near the reference frequency. Because the adaptive notch filter has only one parameter to estimate, the algorithm is simple and easy to control the bandwidth and the depth of zero point, which can accurately track the frequency of interference, and its the stability is guaranteed by limiting the pole to the unit circle [21].

The block diagram of the single frequency adaptive notch filter has 2 adaptive weights as shown in Figure 3. The original input is a mixed waveform $s + n$ of the real signal s and the monochromatic interference n. Besides, the noise and signal are irrelevant. The reference input is a signal x which is not related to the signal, but it is related to noise. The original input is transferred to the d_k end by sampling; the reference input x is sampled to the x_{1k} end and the x_{2k} end. The x_{2k} is a sample value after 90-phase shift of the reference input x, and the purpose is to obtain the two weights of w_{1k} and w_{2k}. Accordingly, the amplitude of the sine wave after the combination can be equal to the amplitude of the interference components in the original input. The weighted output of reference input is y_k, i.e., the estimation of noise n_k, containing the sampling signals d_k and y_k interfering with the frequency. After subtraction, the optimal estimate e_k of useful signals is obtained.

Assuming that the input signal is arbitrary, the reference input is a single frequency sine wave which is expressed as $C\cos(\Omega_0 t + \varphi)$, where Ω_0 in the formula is the angular frequency of the analog signal and C is the amplitude of the reference signal. The original input and the reference input are periodically sampled by the time interval T, while $\omega_0 = \Omega_0 T$ is the sampled signal digital angular frequency. Using the LMS algorithm, the single frequency adaptive notch filter transfer function can be obtained as follows:

$$H(z) = \frac{z^2 - 2z\cos\omega_0 + 1}{z^2 - 2(1 - \mu C^2)z\cos\omega_0 + 1 - 2\mu C^2}. \tag{20}$$

There is zero at frequency f_0, and it is exactly located at $z = e^{\pm j\omega_0}$ of unit flat of Z plane, while the pole is located as follows:

$$z = (1 - \mu C^2)\cos\omega_0 \pm j\left[(1 - \mu C^2) - (1 - \mu C^2)^2 \cos^2\omega_0\right]^{1/2}. \tag{21}$$

The poles in the unit circle, the radial distance of which from the origin is $(1 - \mu C^2)^{1/2}$, approximately equals to $1 - \mu C^2$ so the system is stable. The multifrequency adaptive notch filter is implemented under the parallel structure so that the original input remains to be disturbed signal, and the reference input is expanded into multiple with the amplitude adjusted by 2 weights to realize multiple frequency notch. The output of the adaptive notch filter is the sum of the output of the two-stage notch filter, and the output of the noise canceller is the difference between the original signal input and the output of the adaptive filter. Figure 4 shows that the multifrequency adaptive notch filter is the first notch filter output as the input of the second notch filter, forming a cascade [22].

$$H(z) = H_0(z)H_1(z),$$
$$H_0(z) = \frac{z^2 - 2z\cos\omega_0 + 1}{z^2 - 2(1 - \mu_0 C_0^2)z\cos\omega_0 + 1 - 2\mu_0 C_0^2},$$
$$H_1(z) = \frac{z^2 - 2z\cos\omega_1 + 1}{z^2 - 2(1 - \mu_1 C_1^2)z\cos\omega_1 + 1 - 2\mu_1 C_1^2}. \tag{22}$$

The zero poles of the system are the zero poles of each notch filter, which can directly change the adjustment parameters of one level without affecting the zero pole characteristics of the other notch filter. Therefore, the cascade structure not only has the advantages of the single frequency

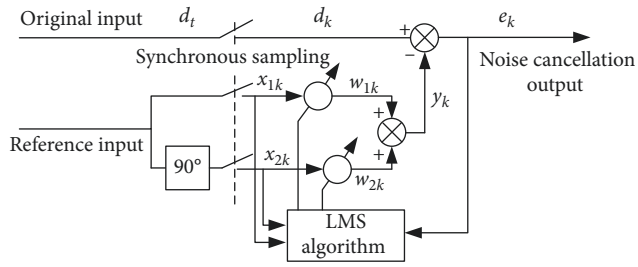

Figure 3: Single frequency adaptive notch filter.

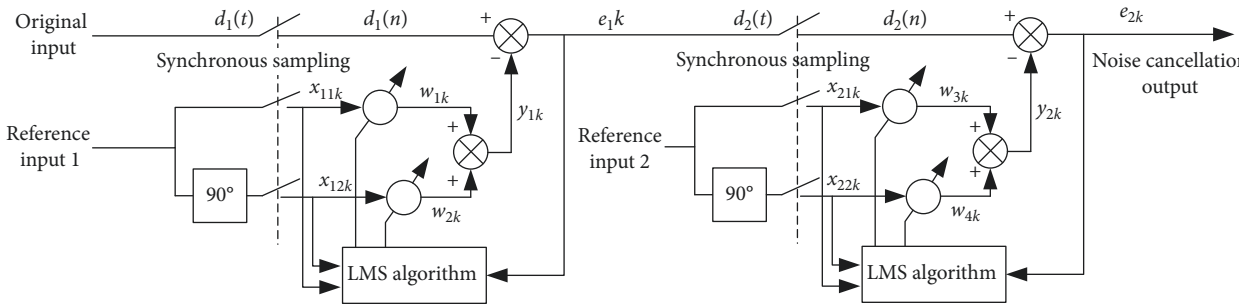

Figure 4: Multifrequency adaptive notch filter.

notch filter but also makes the performance of the notch filter simple and effective and is easier to realize.

4. Simulation Results

In this paper, the frequency response curve of electrohydraulic servo shaking table is measured by using the random wave signal generated by the signal generator. The diagram of resonant suppression is given in Figure 5. The input signal generates a sinusoidal signal with a frequency of resonant frequency ω, and the error signal is obtained under the difference between acceleration signal and acceleration response signal of the electrohydraulic servo shaking table. The LMS adaptive filtering algorithm adjusts the weight of the adaptive notch filter online using the error signal, and the input signal of the adaptive notch filter is weighted by its weight to obtain the output signal. The output signal of the adaptive notch filter serves as the restraining quantity of the resonance. Moreover, the signal added with the input signal serves as new input signal of the shaking table system. After several iterations, the weight of the adaptive notch filter can significantly suppress the resonance, and its amplitude can also be within the required range.

Since the resonance includes resonant peak and resonant valley, the adaptive notch filter must be employed to suppress two targets simultaneously. In this case, it is necessary to input two reference sinusoidal signals, in which the frequency of sinusoidal signals is the frequency of resonant peak and resonant valley. Subsequently, the resonance can be suppressed using the schematic diagram of the resonant suppression, as shown in Figure 5. And the models could be obtained in accordance with previous equation to analyze the performance. The Bode diagram of the open-loop transfer function can be simulated by the noted parameters as shown in Figure 6.

As shown in Figure 7, the low-frequency segment is integral link and two-order oscillation link. As $\omega_L > \omega_0$, the two-order oscillating link is followed by the two-order differential link. The two-order differential link makes the transfer function appear an resonant valley near the natural frequency ω_L of the flexible foundation. And the natural frequency has a cancellation effect on the comprehensive frequency ω_0, which leads to the reduction at ω_0. As $\omega_L < \omega_p$, two-order differential link is followed by a two-order oscillation link. In brief, due to the impact of the elastic load, the frequency of the resonant peak and the resonant valley of the dynamic mechanism are larger than the comprehensive frequency ω_0, which affects the stability of the system. Now given the known K_h, resonant patterns of the system could be used under the different K_L, and the result which is influenced by the multifrequency adaptive notch filter is verified according to the frequency characteristic diagram.

4.1. K_L Is Less than K_h. The load stiffness is relatively small, and the electrohydraulic servo system is mainly based on rigid load. Under the condition of known K_h, the Bode diagram before resonant suppression is shown in Figure 7(a). It is known that resonance occurs at frequencies of 15.9 Hz and 43.8 Hz, respectively. Given the condition of known resonant frequency, the Bode diagram after resonant suppression can be obtained as shown in Figure 7(b).

4.2. K_L Is Similar to K_h. As shown in Figure 8(a) before resonant suppression, resonance is produced at the frequency of 37.4 Hz and 62.1 Hz, and the stability of the system begins to become worse because of the existence of resonance. For the test system, it is necessary to eliminate the coupling effect of the elastic load on the frequency characteristic of the shaking table's acceleration and suppress the

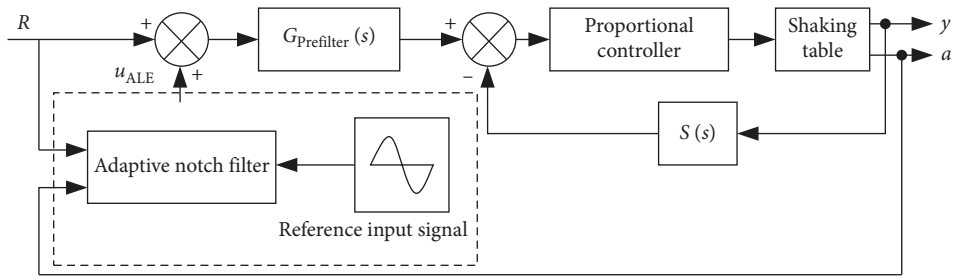

Figure 5: Principle of suppression of the resonance.

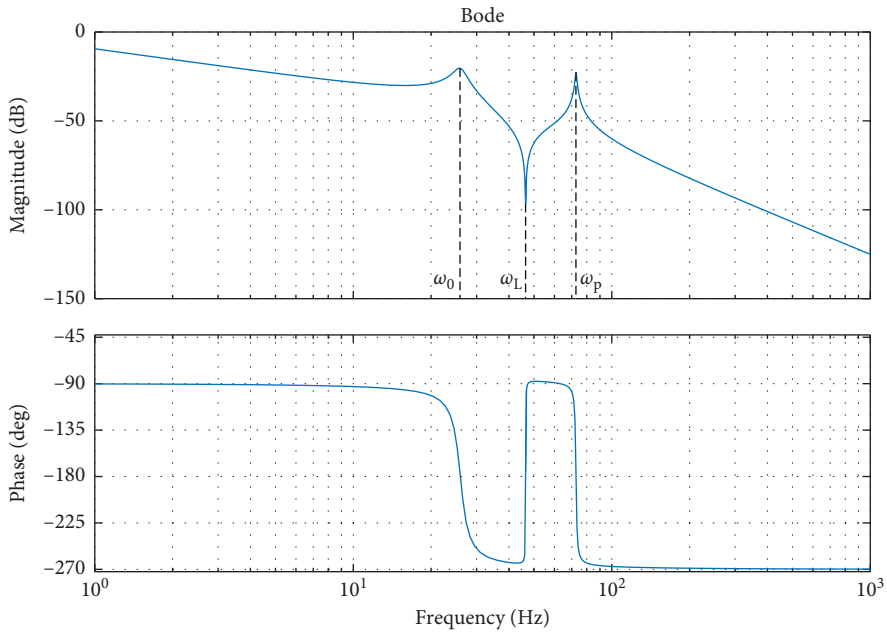

Figure 6: The Bode diagram of the open-loop transfer function under the elastic load.

resonance, so that the frequency characteristic of the shaking table can be in accordance with the performance requirements. The frequency characteristic diagram after resonant suppression is shown in Figure 8(b).

4.3. K_L Is Larger than K_h. Now K_L becomes dominant, and the resonant frequency is larger than before. Figure 9(a) shows the frequency characteristic diagram before resonant suppression for which the frequency points are 50.3 Hz and 77.6 Hz, and Figure 9(b) shows the frequency characteristic diagram after resonant suppression.

Finally, the influence of viscous damping coefficient based on the load of the open-loop transfer function is analyzed, and various damping values are applied for simulation analysis. The values of B_L are 100, 500, and 1000, and other parameters are selected in line with Table 1. As shown in Figure 10 which is the open-loop transfer function, the increase of damping does not impact the comprehensive natural frequency of ω_0, and the frequency value does not change although the value of resonant peak and resonant valley decreases. Accordingly, increasing the viscous damping coefficient of the load can effectively increase the comprehensive damping ratio of the vibration system, whereas it cannot restrain the impact of the resonance.

In this paper, a variety of random vibration power spectrum control strategies are implemented by MATLAB software. In order to compare with others, the same reference power spectrum is used to assess the actual effects of various control techniques including stability, rapidity, accuracy, and other statistical properties. By using the power spectrum, the frequency characteristics should be seen more intuitively.

According to reference power spectrum, digital notch filter and multifrequency adaptive notch filter are used, respectively, to realize the antiresonance. Figure 11 shows that the frequency of resonance is 16.6 Hz and 44.3 Hz. Because of the resonant effect, the frequency response is not satisfactory. Its result is suppressed using digital filter depicted in Figure 12. Figure 13 is the resonant suppression using multifrequency adaptive notch filter. The comparison of the two methods shows that the traditional digital notch filter can ensure precision of control process, but small feedback gain leads to a relatively slow convergence process, and the excessive feedback gain easily leads to the divergence of the control process.

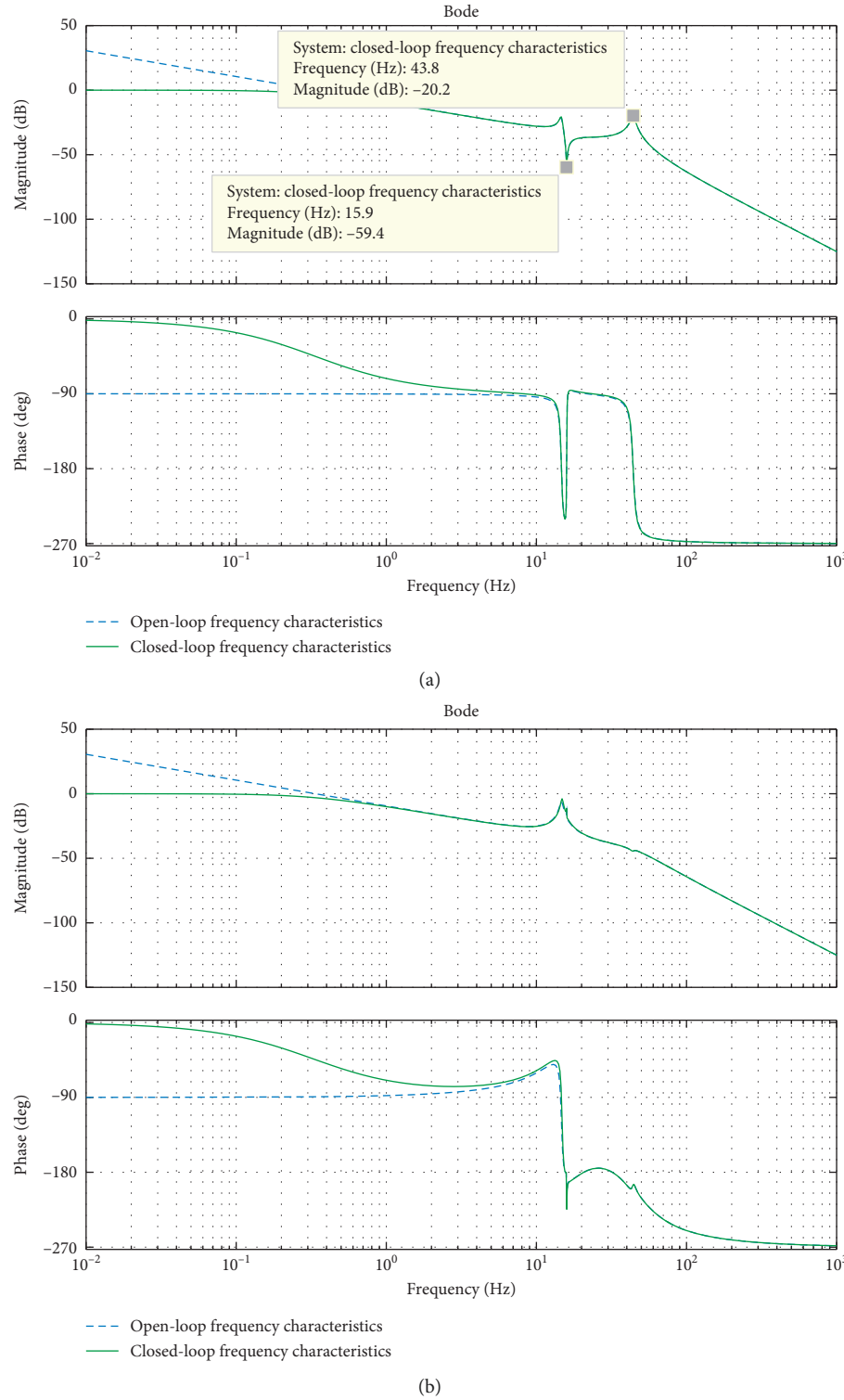

Figure 7: Frequency characteristic diagrams of the system: (a) before resonant suppression; (b) after resonant valley suppression.

The accuracy of the traditional digital notch filter can only reach the tolerance requirement of ±3 dB, and the maximum deviation occurs at the resonance point, but the multifrequency adaptive notch filter achieves an accuracy of ±3 dB after several iterations. The main reason for improving the precision is that the adaptive control can allow the increase of the feedback gain no matter what causes the instability of the system. That is to say, the adaptive control algorithm can keep the stability of the iterative process and also has control precision.

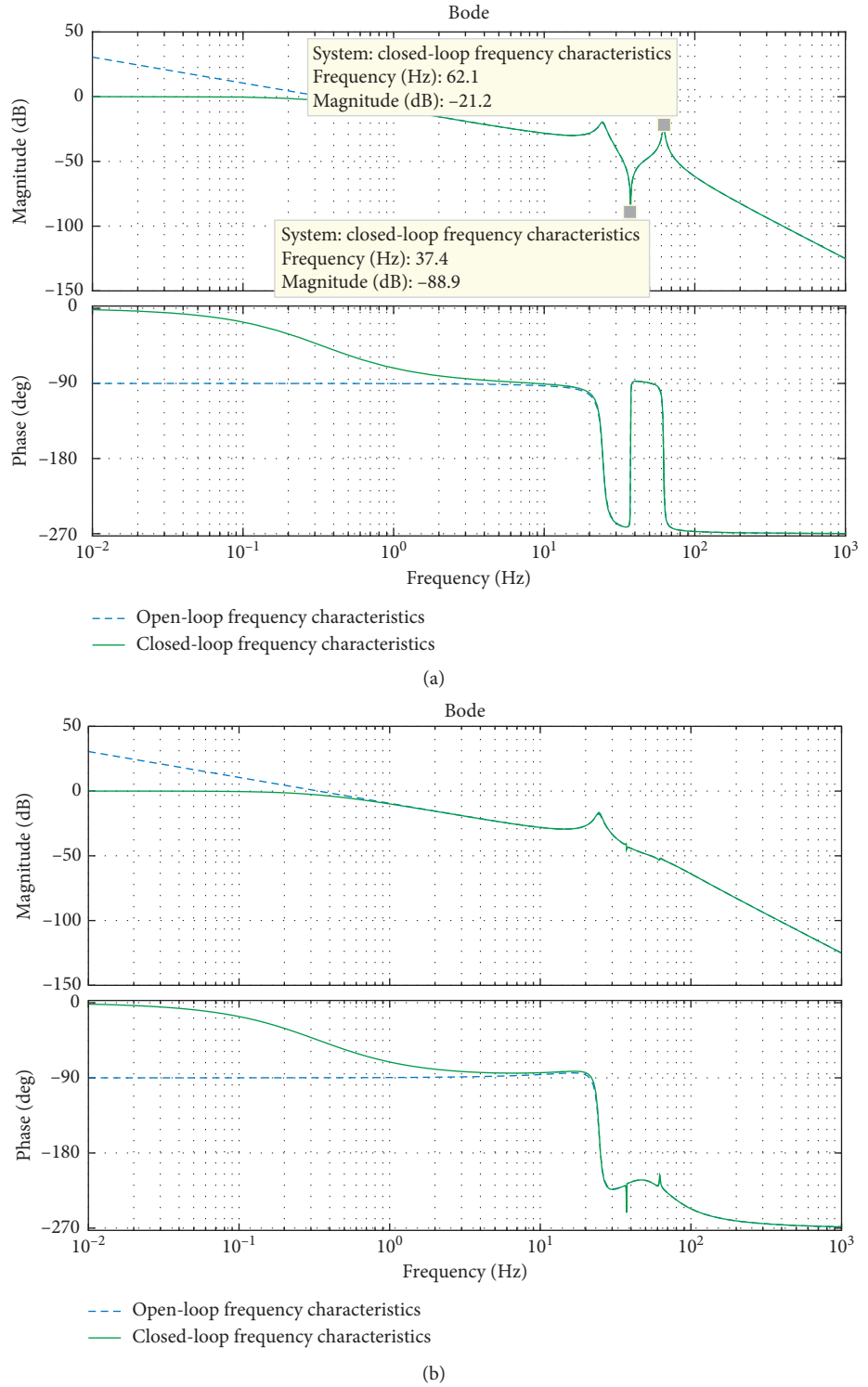

Figure 8: Frequency characteristic diagrams of the system: (a) before resonant suppression; (b) after resonant suppression.

5. Conclusions

In this paper, when the shaking table is elastic load, the coupling action between elastic load and the hydraulic system constitutes an elastic load-resonant system. In this case, the servo system is analyzed by establishing the mathematical model, and the bandwidth can be improved by adding three-variable controller. To suppress the resonance of the shaking table at the frequency of the trap, we propose a multifrequency adaptive notch filter suppression strategy

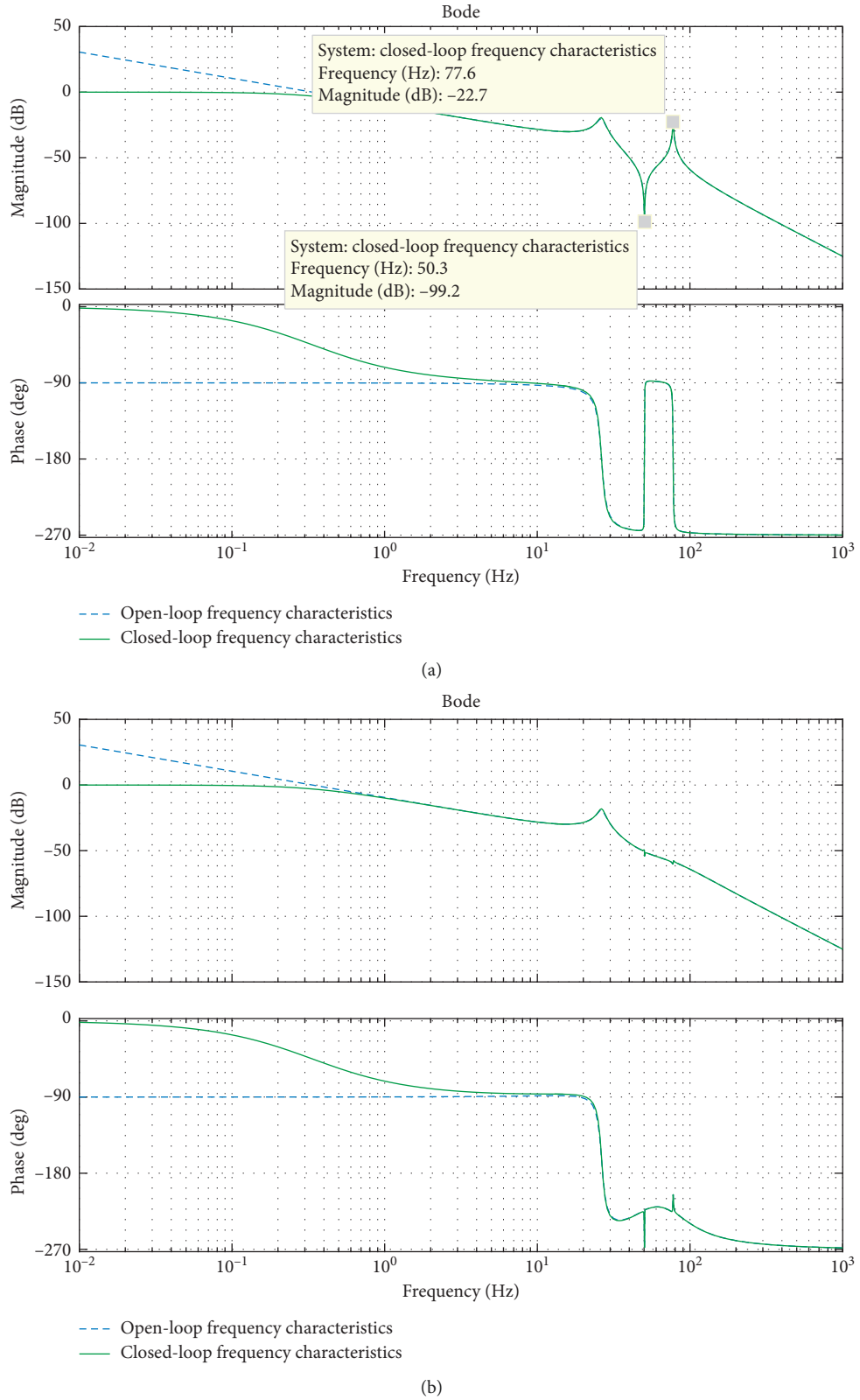

Figure 9: Frequency characteristic diagrams of the system: (a) before resonant suppression; (b) after resonant suppression.

based on the LMS algorithm by studying the resonant frequency and the frequency characteristic of the adaptive trap at the zero point in the unit circle. Considering the different load stiffness, MATLAB simulates the resonant suppression and verifies the effectiveness of multifrequency adaptive notch filter.

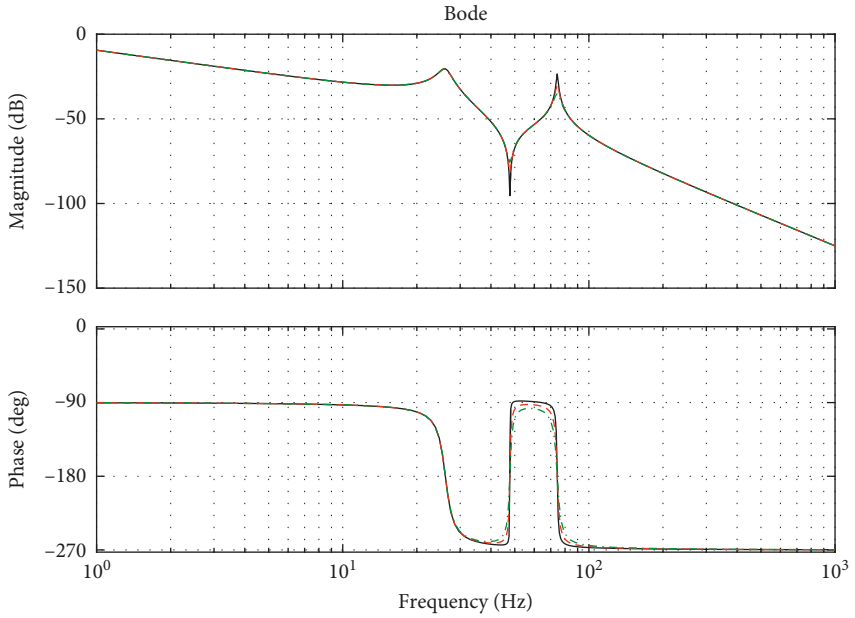

Figure 10: The open-loop Bode diagram of different viscous damping coefficients of load.

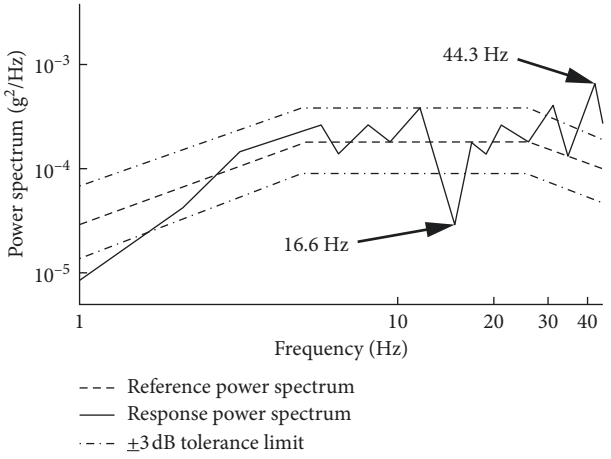

Figure 11: Before resonant suppression.

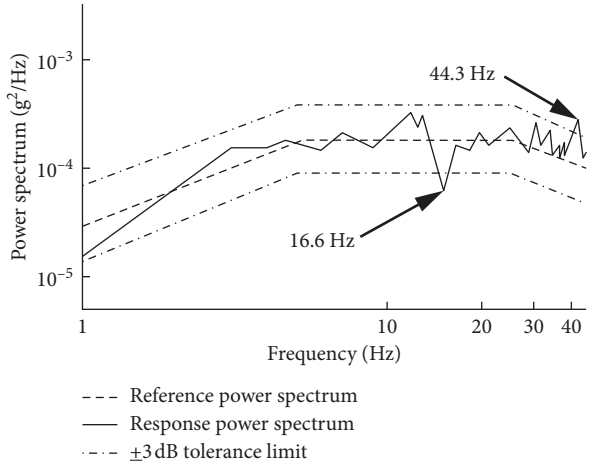

Figure 12: After resonant suppression by the digital filter.

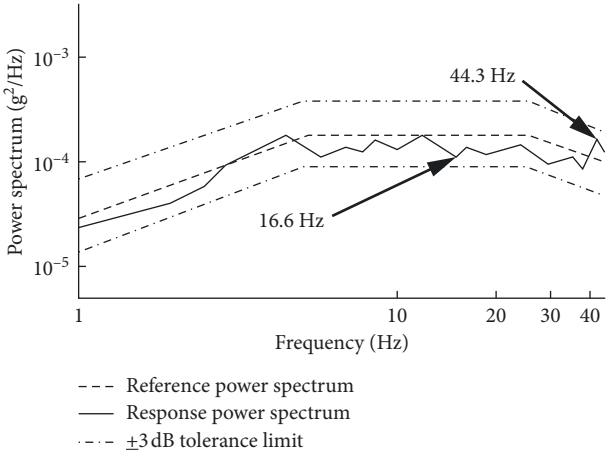

Figure 13: After resonant suppression by the multifrequency adaptive notch filter.

In this study, the random vibration control is conducted, and the results suggest that the multifrequency adaptive notch filter has better stability, quicker convergence speed, and higher precision than traditional notch filter. Also, the multifrequency adaptive notch filter meets requirements of the stability of the random process. Besides, it is suggested from the results that this control mode has high control accuracy and real-time performance for different frequency bands and different system characteristics and has high application value.

Notations

A: Effective area of the hydraulic cylinder piston
B_L: Viscous damping coefficient of the piston and load
C: Amplitude of the reference signal

C_{tp}: Total leakage coefficient of the hydraulic cylinder
K_c: Flow-pressure coefficient
K_{ce}: Total flow-pressure coefficient
K_h: Hydraulic spring stiffness
K_L: Spring stiffness of the load
K_q: Flow gain
m_L: Elastic load quality
m_p: Equivalent mass of the load inertia
p_i: The pressure in the oil inlet of the hydraulic cylinder
p_L: Load voltage drop
p_o: The pressure in the oil outlet of the hydraulic cylinder
q_i: Flow into a hydraulic cylinder
q_L: Load flow
q_o: Flow out of the hydraulic cylinder
V_i: The volume of the hydraulic cylinder
V_o: The volume of the hydraulic cylinder
V_t: The total volume of the two chamber of the hydraulic cylinder
x_v: Spool displacement
y: Hydraulic cylinder displacement
y_L: Load displacement
y_p: Piston displacement
β_e: Equivalent bulk modulus of elasticity
ω_0: Synthetic frequency
ω_h: The natural frequency of power mechanism
ω_L: The frequency of resonant valley
ζ_L: Damping value of resonant valley
ω_p: The frequency of resonant peak
ω_x: Coupling frequency
ζ_x: Coupled damping value.

Data Availability

The figures and equipment parameters data used to support the findings of this study are included within the article.

Conflicts of Interest

The authors declare no potential conflicts of interest with respect to the research, authorship, and/or publication of this article.

Acknowledgments

This project was supported by the HTC3250μn Precision NC Lathe and Turning Center, which is a subproject attached to the National Science and Technology Major Project (2009ZX04001-053).

References

[1] R. T. Severn, "The development of shaking tables-a historical note," *Earthquake Engineering & Structural Dynamics*, vol. 40, no. 2, pp. 195–213, 2011.

[2] S. Matthew and N. Narutoshi, "Direct acceleration feedback control of shake tables with force stabilization," *Journal of Earthquake Engineering*, vol. 17, no. 5, pp. 736–749, 2013.

[3] A. R. Plummer and P. S. Guinzio, "Modal control of an electrohydrostatic flight simulator motion system," in *Proceedings of ASME Dynamic Systems and Control Conference (DSCC 2009)*, pp. 1257–1264, American Society of Mechanical Engineers, Hollywood, CA, USA, October 2009.

[4] A. R. Plummer, "High bandwidth motion control for multi-axis servohydraulic mechanisms," in *Proceedings of 2007 ASME International Mechanical Engineering Congress and Exposition*, pp. 1–7, American Society of Mechanical Engineers, Seattle, WA, USA, November 2007.

[5] N. E. Earnhart and K. A. Cunefare, "Compact Helmholtz resonators for hydraulic systems," *International Journal of Fluid Power*, vol. 13, no. 1, pp. 41–50, 2012.

[6] H. L. Wang, G. L. Tian, L. F. Fu, G. Qiang, and W. Q. Zhao, "Study on resonance of braking pressure control system of multi-wheel and multi-strut aircraft," *Journal of Northwestern Polytechnical University*, vol. 34, no. 6, pp. 646–650, 2014.

[7] J. L. Lu, C. H. Yuan, and J. Sun, "A method of weakening the resonant of the aircraft brake pressure control system," *Machine Tool and Hydraulic*, vol. 44, no. 13, pp. 44–47, 2016.

[8] Y. L. Fu, W. Q. Luo, and M. X. Wang, "Servo controller design of multi-stage system for low-frequency resonance rejection," *Chinese Hydraulics and Pneumatics*, vol. 23, no. 12, pp. 58–62, 2010.

[9] S. Tomoki, T. Kenta, U. Koudai, S. Sho, and T. Toshiaki, "Modeling and resonance suppression control for electro-hydrostatic actuator as a two-mass resonant system," *Advanced Robotics*, vol. 32, no. 1, pp. 1–11, 2018.

[10] G. W. Younkin, "Compensating structural dynamics for servo driven industrial machines with acceleration feedback," in *Proceedings of 2004 IEEE Industry Applications Conference: 39th IAS Annual Meeting*, pp. 1881–1890, Institute of Electrical and Electronics Engineers Inc., Seattle, WA, USA, October 2004.

[11] Y. Z. Cao, S. D. Lan, W. R. Wu, and L. Lou, "Study on vibration cylinder resonance suppression of electro-hydraulic shaking table," *Computer Simulation*, vol. 33, no. 12, pp. 193–197, 2016.

[12] Y.-Q. Wang, F.-C. Huang, and H.-B. Liu, "Adaptive filtered x-least mean square algorithm with improved convergence for resonance suppression," *Proceedings of the Institution of Mechanical Engineers, Part I: Journal of Systems and Control Engineering*, vol. 228, no. 9, pp. 668–676, 2014.

[13] C.-I. Kang and C.-H. Kim, "An adaptive notch filter for suppressing mechanical resonance in high track density disk drives," *Microsystem Technologies*, vol. 11, no. 8–10, pp. 638–652, 2005.

[14] N. Li and S. H. Li, "Suppression of servo system mechanical resonance based on adaptive IIR notch filter," in *Proceedings of the 2015 27th Chinese Control and Decision Conference*, pp. 3418–3423, Institute of Electrical and Electronics Engineers Inc., Qingdao, China, May 2015.

[15] W. Bahn, T.-I. Kim, S.-H. Lee, and D.-I. D. Cho, "Resonant frequency estimation for adaptive notch filters in industrial servo systems," *Mechatronics*, vol. 41, pp. 45–57, 2017.

[16] M. Yang, L. Hao, and D. G. Xu, "Online suppression of mechanical resonance based on adapting notch filter," *Journal of Harbin Institute of Technology*, vol. 46, no. 4, pp. 63–69, 2014.

[17] P. J. C. Branco and J. A. Dente, "Design and experimental evaluation of a fuzzy logic pressure controller for the Airbus 310/320 braking control system," *Engineering Applications of Artificial Intelligenc*, vol. 23, no. 6, pp. 989–999, 2010.

[18] H. R. Li, *Hydraulic Control System*, National Defense Industry Press, Beijing, China, 1990.

[19] C. X. Wang, *Hydraulic Control System*, Machinery Industry Press, Beijing, China, 1990.

[20] J. T. Guan, *Electro-Hydraulic Control Technology*, Tongji University Press, Shanghai, China, 2003.
[21] T. Linder, H. Zojer, and B. Seger, "Fully analogue LMS adaptive notch filter in BiCMOS technology," *IEEE Journal of Solid-State Circuits*, vol. 31, no. 1, pp. 61–69, 1996.
[22] M. K. Biswal, P. K. Dash, and S. Nanda, "Multi-harmonic frequency identification through multistage adaptive notch filter and least squares," in *Proceedings of 2011 International Conference on Energy, Automation and Signal (ICEAS)*, pp. 726–729, IEEE, Bhubaneswar, Odisha, India, December 2011.